Massive MIMO Interference Coordination for 5G Broadband Access: Integration and System Level Study

A. Grassi[a,b], G. Piro[a,b,*], G. Boggia[a,b], M. Kurras[c], W. Zirwas[d], R. SivaSiva Ganesan[d], K. Pedersen[e], L. Thiele[c]

[a]*Politecnico di Bari, v. Orabona 4, 70125 Bari, Italy*
[b]*CNIT, Consorzio Nazionale Interuniversitario per le Telecomunicazioni*
[c]*Fraunhofer Heinrich Hertz Institute, Einsteinufer 37, 10587 Berlin, Germany*
[d]*Nokia Bell Labs, Werinherstrasse 91, 81541 Munich, Germany*
[e]*Nokia Bell Labs, NOVI-6 Alfred Nobels Vej 21C, DK-9220 Aalborg East, Denmark*

Abstract

Upcoming 5G systems are called to face a huge growth of mobile traffic compared to the current 4G technology. To meet this challenge, the Massive Multiple-Input Multiple-Output (mMIMO) emerged as an essential and capable transmission technique, able to concurrently serve a large number of users, while guaranteeing a very high spectral efficiency. Moreover, some other additional approaches, like the Joint Spatial Division and Multiplexing precoding scheme and the multi-cell coordinated beamforming technique for interference reduction, could be used to further improve the overall system performance and reduce the mMIMO implementation complexity. Unfortunately, the current scientific literature does not provide a clear overview on how and in which conditions these mechanisms can be successfully harmonized, configured, and adopted in real 5G deployments. To bridge this gap, this paper deeply investigates the configuration and the integration of these promising transmission techniques. Moreover, it also evaluates, from the system level perspective, their behavior in different operating conditions. From one side, obtained results clearly show the

---

[*]Corresponding author
Email addresses: `alessandro.grassi@poliba.it` (A. Grassi), `giuseppe.piro@poliba.it` (G. Piro), `gennaro.boggia@poliba.it` (G. Boggia), `martin.kurras@hhi.fraunhofer.de` (M. Kurras), `wolfgang.zirwas@nokia-bell-labs.com` (W. Zirwas), `rakash.sivasivaganesan@nokia-bell-labs.com` (R. SivaSiva Ganesan), `klaus.pedersen@nokia-bell-labs.com` (K. Pedersen), `lars.thiele@hhi.fraunhofer.de` (L. Thiele)

performance gain that these new techniques offer with respect to the existing 4G technology. From another side, however, they also identify the scenarios where the proper combination of these emerging techniques is really fruitful for meeting the expected quality requirements defined for the 5G.

1. Introduction

The 5th Generation (5G) of cellular networks is being developed with the ambitious goal to support a very heterogeneous mixture of services, each with its own specific requirements. In this context, the enhanced Mobile Broadband (eMBB) use case is always under the reflectors of the worldwide research community, because it embraces many mature services with high bandwidth requirements, such as video streaming, work collaboration, and cloud storage [1]. Recently, eMBB was upgraded with an increasingly large capacity. Specifically, to provide a satisfactory quality level to its common applications, the required data rate is estimated to be at least equal to 50 Mbps [2][3]. This is intended as the real perceived throughput that should be supplied to each user, rather than the theoretical peak rate in ideal conditions. The traffic density, defined as the ratio between the throughput registered in a given area and the geographical extension of that area, can easily reach values of many Gbps [4]. The exact value is directly proportional to the user density: for example, for a density of 100, 400, or 2500 users/km^2, the required traffic density amounts to 5, 20, or 125 Gbps/km^2 [4].

Massive MIMO (mMIMO) is a very promising concept, introduced to enhance the performance of wireless networks, including the upcoming 5G technology. It mainly leverages a very large number of independently controllable antennas at the base station [5], thus achieving great improvements in terms of spectral and energy efficiency [6, 7].

mMIMO was natively conceived to work in a Time Division Duplexing (TDD) operation mode [5] [7] [6]. But, its adoption in communication technologies operating in Frequency Division Duplexing (FDD) mode (like the current and upcoming mobile networks), is now under investigation [8][9][10][11][12]. Moreover, additional techniques can be used to further improve mMIMO performance, while reducing its implementation complexity.

For instance, in the context of the European H2020 FANTASTIC-5G project [13], two promising transmission techniques were identified, with the purpose of enhancing the performance of macro-cellular mobile networks and push them towards the 5G expectations. The first one is the Joint Spatial Division and Multiplexing (JSDM) technique. It aims at creating major beamforming and multiplexing gains, allows a simpler implementation of the baseline mMIMO approach, and ensures a native compatibility with FDD systems [12]. The second one is the inter-cell coordinated beamforming method, firstly proposed in [14]. It can be implemented on top of an mMIMO+JSDM infrastructure with very little inter-site communication, with the aim of reducing the average interference level and further increasing the throughput.

At the time of this writing, these techniques have been evaluated at the link-level perspective [14, 15, 16] and only few contributions provided preliminary analysis of mMIMO at the system level [17, 18, 19, 20]. But, for the best of the authors' knowledge, the current literature presents many limitations. First, it is not clear how and in which conditions mMIMO+JSDM and coordinated beamforming techniques can be successfully harmonized, configured, and adopted. Second, available studies generally consider simplified assumptions that are too far from concrete 5G deployments. Third, the coordinated beamforming scheme presented in [14] doesn't work properly in a multi-cell environment.

Starting from these premises, the work presented herein deeply investigates the configuration and the integration of mMIMO-based transmission techniques in concrete 5G deployments. Moreover, it evaluates, from the system level perspective, their behavior in different operating conditions. It is worth to emphasize that this paper should not be simply intended as a survey-like study

of well-known approaches. Instead, it offers an important step forward for the current state of the art because it deeply investigas mMIMO-based transmission strategies properly set for concrete 5G deployments, reports new results not yet available in the current scientific literature, and provides concrete answers to the aforementioned pending issues.

To this end, we integrate mMIMO in the open-source LTE-Sim simulator [21], which features a complete network stack including, e.g., the Medium Access Control (MAC) layer, the packet scheduler and the link adaptation process. We also develop the coordinated beamforming as an optional additional feature, while improving and optimizing the original design for a full multi-cell environment. The resulting tool is used to compare the mMIMO technique (implemented with the JSDM approach, and optionally with coordinated beamforming) against a baseline Long Term Evolution Advanced (LTE-A) technology, in a variety of operating scenarios, which are defined in terms of user density and Inter-Site Distance (ISD), ranging from ultra-dense urban deployments (2500 users/km^2 with 200 m ISD) to low-density rural areas (100 users/km^2 with 1000 m ISD). In the FANTASTIC-5G project's terminology, these scenarios correspond to the "Dense Urban Society" and "50 Mbps Everywhere" use cases [22]. By measuring Key Performance Indicators (KPIs), such as user experienced data rate, traffic density, and cell throughput (all of which are rigorously defined later in Sec. 5.2), we try to ascertain whether the 5G requirements can be addressed with the presented technologies. The resulting answer is revealed to be positive when reasonable deployment conditions are taken into account. In particular, the throughput provided with the investigated approaches is about twice the required value. The most advanced solution (mMIMO with coordinated beamforming) can provide a throughput gain of about 550%-850% compared to the baseline, and 10%-20% compared to the mMIMO alone.

Moreover, a further investigation on Channel State Information (CSI) acquisition demonstrated that a minimal throughput reduction is achieved even if mobile terminal are configured to discard the less relevant components from the CSI feedback reporting.

The rest of this paper is organized as follows: Sec. 2 discusses the existing literature on the subject, while Sec. 3 provides notations and the general system model, and Sec. 4 gives more details on the evaluated technologies. Sec. 5 presents the results and related discussions. Finally, Sec. 6 draws the conclusions.

2. Literature review

Massive MIMO (mMIMO) is a very promising transmission technique, introduced to enhance the performance of wireless networks. It mainly leverages a very large number of independently controllable antennas at the base station [5], thus achieving great improvements in terms of spectral and energy efficiency [6]. When implemented in TDD or FDD configurations, it offers a different set of advantages and disadvantages. Starting from an overview of the current state of the art and a joint comparison of available solutions, this Section clearly illustrates the motivations that are at the basis of this work.

2.1. Implementation of mMIMO in TDD mode

Many works focusing on mMIMO assume a TDD operation to only perform channel estimation in the uplink direction, and then exploit channel reciprocity and use the acquired CSI for the downlink as well [7]. This has the advantage that the CSI estimation overhead is proportional to the number of active users, rather than the much higher number of downlink antennas. The use of TDD has been proposed since the seminal papers on mMIMO, and the basics remain basically unchanged as long as the TDD mode is maintained. Various proposals are built on top of it, such as the use of 1-bit analog-to-digital converters to reduce hardware costs [23], hardware calibration to ensure true uplink-downlink reciprocity [24], and channel modeling with large antenna arrays [25].

When mMIMO is implemented in TDD mode, an important concern is the pilot contamination effect. Specifically, it arises from the limited number of available uplink training sequences, with the subsequent necessity to reuse them

5

at relatively short distances [26]. Differently from other issues, such as fast fading and inter-user interference, pilot contamination persists even if the number of base station antennas grows to infinity. Therefore, it must be approached by other means [27]. At the time of this writing, interesting techniques have been presented in [26], [28], [29] and [30]. In [26], the problem is solved by introducing a multi-cell MMSE precoding approach, which considers the training sequences allocated to all the terminals. The authors of [28] describe a pilot contamination precoding technique that involves multiple cells, but only requires knowledge of the slow-fading coefficients from the other cells. The work in [29] proposes a time-shifting of the pilot signals transmission in different cells, on the basis that non-overlapping transmissions (in time) of the same pilot do not cause contamination. Recently, [30] proposed software-defined mMIMO, which employs coordination of multiple remote radio heads, each one with a large number of antennas.

2.2. Implementation of mMIMO in FDD mode

Most of the 4th Generation (4G) network deployments currently operate in FDD mode, and converting them to TDD is not straightforward. Emerging 5G networks will still operate in FDD mode. Therefore, it can be desirable to adapt mMIMO to FDD operation as well. This task is not easy to accomplish. First, with a typical pilot-based channel estimation, the overhead would be proportional to the number of base station antennas. Thus, a simple mMIMO implementation could quickly become infeasible [31]. Second, the CSI about the downlink channel should be explicitly fed back to the base station, and there is a trade-off between CSI precision and utilization of the limited uplink resources [32]. In fact, in FDD mMIMO, the problem of CSI acquisition becomes much more severe than pilot contamination. Thus, it is generally tackled first, and then pilot contamination is considered in the resulting system, if necessary. However, most strategies proposed to reduce the CSI overhead work by reducing the dimensionality of the channel, which has the positive side effect of reducing the number of required pilots, as well as the pilot contamination effect itself.

The literature proposes different methods to achieve an FDD-based mMIMO system. For example, [8] describes a technique to reduce the number of required training signals by exploiting spatially correlated channels. The work in [9] presents a framework based on Compressive Sensing to collect only partial CSI information at the users and reconstruct the entire channel matrix at the base station, and the idea is further extended in [10]. Also, [11] proposes training schemes with memory, which use not only the last received training signal but also previous ones. In [33], the author propose a codebook-based feedback quantization with linear (rather than exponential) search complexity. The works in [34, 35] describe a feedback scheme for beamforming-based networks where only relevant components of relevant beams are reported, resulting in high accuracy and low overhead.

The Joint Spatial Division and Multiplexing (JSDM) is described in [12]. It is a two-stage precoding approach: while the first-stage precoder captures the long-term second-order statistics of the channel and reduces the CSI size (both for estimation and uplink feedback), the second-stage precoder captures the short-term channel variations. As stated in [12] a near-optimal choice for the first-stage precoder is a set of unitary Discrete Fourier Transform (DFT) vectors. This configuration is usually referred to as a Grid-of-Beams (GoB), because it produces a number of spatially-oriented beams. As for the second-stage precoder, any standard Multi-User MIMO (MU-MIMO) strategy can be used, including linear filters such as Maximum Ratio Transmission (MRT) and Regularized Zero Forcing (RZF)[36]. With suitable parameters, this strategy reduces the size of the "effective" channel (i.e. as seen after the first-stage precoding) so that the amount of pilot signals and CSI feedback are decreased as well. Moreover, each user only receives a subset of the produced beams with relevant intensity, leaving room for further savings as explained in [37]. Initially studied for a single-cell scenario, the JSDM framework is investigated in a multi-cell fashion in [14] with promising results. However, the analysis only considers a cluster of 3 adjacent sectors from different sites, which does not directly extend to a complete multi-cell scenario. Such a configuration is properly taken into

account in the present work.

Few studies can be found in the literature which evaluate the performance of mMIMO in a network based on FDD at the system level, in terms of user and/or cell throughput. One such work is [17], where a multiple types of antenna arrays are evaluated against a baseline Release 8 Long-Term Evolution (LTE) system. However, it uses a simple MRT criterion for the transmission beamforming, and the problem of downlink training overhead is not discussed. Moreover, only a single scenario (in terms of user density and ISD) is investigated. Finally, the baseline setup is only a 2x2 Multiple-Input Multiple-Output (MIMO) system, which is quite out-of-date with respect to current LTE-A capabilities.

A similar evaluation is presented in [18], which also compares multiple antenna array geometries. While this study adds the effect of different user densities, it presents limitations similar to the previous one. Specifically, no measure is taken to reduce the overhead of channel estimation, and the effect of different ISDs is not discussed. Also, no baseline solution is used as a comparison term.

3rd Generation Partnership Project (3GPP) carried out a calibration study for Full Dimension MIMO (FD-MIMO) in LTE [19], using 2D arrays for elevation as well as azimuth beamforming. However, the assumptions include a smaller number of antennas and a feedback scheme based on LTE codebooks. There is also an ongoing calibration study for beamforming in 5G [20], but only one User Equipment is scheduled at any given time.

2.3. Final considerations

To provide a further insight, an overview of advantages and disadvantages characterizing the implementation of mMIMO in both TDD and FDD modes is reported in Table 1. By jointly considering the advantages offered by mMIMO operating in a FDD mode and the deployment features of upcoming 5G networks, it is easy to accept that technical components implementing mMIMO in FDD emerge as the most promising approaches. However, the limitations affecting the solutions and the preliminary studies already available in the current scientific literature and the disadvantages reported in Table 1 pave the

8

TDD operation mode	
Pros	No need for downlink training.
	Uplink training overhead only grows as the number of users.
	UL/DL reciprocity can be exploited.
Cons	Simple training schemes suffer from pilot contamination.
	Many networks operate as FDD, conversion is expensive.
	Reciprocity can be hindered by hardware impairments.

FDD operation mode	
Pros	Compatible with lots of existing spectrum licences and equipment.
	Many techniques for CSI overhead reduction are being investigated.
	Such techniques also help with pilot contamination.
Cons	Simple pilot-based training incurs large overhead.
	Needs both downlink training and uplink feedback.

Table 1: Advantages and disadvantages related to the implementation of mMIMO in both TDD and FDD modes.

way for new research contributions. This represents a clear motivation for the importance that the present work has for the current state of the art.

3. System Model

3.1. Notations

Throughout this paper, we use calligraphic uppercase letters to designate a set of indices, where $\mathcal{A} = \{1, \ldots, A\}$, and $A = |\mathcal{A}|$ denotes the cardinality of the set. Consequently, upper and lower case letters denote a scalar. In contrast to this, boldface lower-case letters and boldface upper-case letters are used to represent column vectors and matrices, respectively. The element of a matrix is indicated by $[\mathbf{A}]_{i,j}$, where the first subscript means the i-th row and the second subscript the j-th column of matrix $\mathbf{A}$. The element of a vector is indicated by $[\mathbf{a}]_i$. The A-dimensional identity matrix is given by $\mathbf{I}_A$. Moreover, $(\cdot)^*$, $(\cdot)^{\mathrm{T}}$, and

$(\cdot)^{\mathrm{H}}$ denote complex conjugate, transpose, and complex conjugate transpose of a vector or matrix. The trace of a square matrix $\mathbf{A}$ of size $A \times A$ is defined as $\mathrm{trace}\,(\mathbf{A}) = \sum_{a=1}^{A} [\mathbf{A}]_{a,a}$. $\sqrt{(\cdot)}$ denotes the element-wise square root and $\mathbb{E}\,[\cdot]$ is the expectation operation.

In order to improve the readability of this manuscript, the list of mathematical symbols adopted herein is summarized in Table 2.

3.2. Description

In this work we consider a multi-cell network architecture, based on the Orthogonal Frequency Division Multiplexing (OFDM) physical layer. More specifically, the communication between base stations and mobile terminals, simply referred to as downlink, is taken into account. The considered scenario integrates K mobile terminals and L base stations. Therefore, let $\mathcal{K} = \{1, \ldots, K\}$ and $\mathcal{L} = \{1, \ldots, L\}$ be the list of mobile terminals and base stations available in the network. Furthermore, each base station $l \in \mathcal{L}$ is equipped with M antennas and each device $k \in \mathcal{K}$ with N antennas.

Focusing the attention to the k-th mobile terminal, let $\mathbf{y}_k \in \mathbb{C}^N$ be the received signals at the N antennas. It is expressed as:

$$\mathbf{y}_k = \sum_{l \in \mathcal{L}}^{} \mathbf{H}_{k,l}\sqrt{\mathbf{P}_l}\mathbf{V}_l\mathbf{x}_l + \mathbf{n}_k, \tag{1}$$

where, $\mathbf{H}_{k,l} \in \mathbb{C}^{N \times M}$ is the channel matrix between the l-th base station and the k-th device, $\mathbf{P}_l \in \mathbb{R}^{M \times M}$ is a diagonal power allocation matrix with the sum constraint $\mathrm{trace}\,(P) \leq P_{\max}$, $\mathbf{V}_l \in \mathbb{C}^{M \times T_l}$ denotes the downlink precoding matrix of the l-th base station, $\mathbf{x}_l \in \mathbb{C}^{T_l}$ are the transmitted symbols of the l-th base station and $\mathbf{n}_k \sim \mathcal{CN}\left(0, \sigma^2\mathbf{I}_N\right)$ constitutes the Gaussian distributed uncorrelated noise with variance σ^2. The parameter T_l represents the number of spatial multiplexed stream/layers of the l-th base station. Under the assumption that stream t from the l-th base station is allocated to the k-th device, the

Table 2: Symbol reference

Symbol	Meaning
$\mathcal{L}$	Set of base stations in the system
$\mathcal{K}$	Set of mobile terminals in the system
$\mathcal{T}_l$	Set of streams transmitted by the l-th base station
$\mathbf{x}_l$	Signal transmitted from the l-th base station
$\mathbf{V}_l$	Precoding matrix of the l-th base station
$\mathbf{B}_l$	First-stage precoder of the l-th base station
$\mathbf{b}_{l,i}(k)$	Precoder to produce the i-th beam using k antennas
$\mathbf{C}_l$	Second-stage precoder of the l-th base station
$\mathbf{D}_l$	Non-normalized RZF precoding matrix
$\mathbf{E}_l$	Power normalization matrix
$\mathbf{P}_l$	Power allocation matrix of the l-th base station
$\mathbf{H}_{k,l}$	Channel matrix from the l-th base station to the k-th mobile terminal
$\mathbf{H}_l$	Channel matrix from the l-th base station to all its served mobile terminals
$\mathbf{y}_k$	Signal received by the k-th mobile terminal
$\mathbf{n}_k$	Receiver noise at the k-th mobile terminal
$\tilde{\mathbf{h}}_{k,t}$	Effective signal of the t-th stream at the k-th mobile terminal
$\tilde{\vartheta}_{k,t}$	Intra-cell interference for the t-th stream at the k-th mobile terminal
$\tilde{\mathbf{z}}_k$	Inter-cell interference at the k-th mobile terminal
$\tilde{\mathbf{w}}_{k,t}$	Receiver filter for the t-th stream at the k-th mobile terminal
$\mathbf{W}_l$	Estimated compound receive filter of all the mobile terminals served by the l-th base station
$\gamma_{k,t}$	Receive Signal-to-Interference-plus-Noise Ratio (SINR) for the t-th stream at the k-th mobile terminal
σ^2	Thermal noise variance

received signal in Eq. (1) can be rewritten as:

$$\mathbf{y}_{k,t} = \underbrace{\mathbf{H}_{k,l}\sqrt{p_t}\mathbf{v}_{t,l}x_{t,l}}_{\tilde{\mathbf{h}}_{k,t}} + \underbrace{\sum_{\substack{j \neq t}}^{j \in \mathcal{T}_l} \mathbf{H}_{k,l}\sqrt{p_j}\mathbf{v}_{j,l}x_{j,l}}_{\boldsymbol{\vartheta}_{k,t}}$$
$$+ \underbrace{\sum_{\substack{m \neq l}}^{m \in \mathcal{L}} \mathbf{H}_{k,m}\sqrt{\mathbf{P}_m}\mathbf{V}_m\mathbf{x}_m + \mathbf{n}_k}_{\mathbf{z}_k}, \tag{2}$$

where $\mathcal{T}_l = \{1, \ldots, T_l\}$ is the set of stream indices for the l-th base station. In Eq. 2, the received signal is divided into three parts: the effective signal corresponding to the t-th stream is reported in $\tilde{\mathbf{h}}_{k,t}$; the intra-sector interference caused by streams $j \neq t$ from the l-th base station is reported in $\boldsymbol{\vartheta}_{k,t}$; and finally inter-sector interference plus noise is denoted by $\mathbf{z}_k$.

Under the assumption of Gaussian distributed symbols and an equalizer or combiner denoted by $\mathbf{w}_{k,t} \in \mathbb{C}^N$, the SINR of the received signal in Eq. 2, that is $\gamma_{k,t}$, is expressed as:

$$\gamma_{k,t} = \frac{\mathbf{w}_{k,t}^{\mathrm{H}}\tilde{\mathbf{h}}_{k,t}\tilde{\mathbf{h}}_{k,t}^{\mathrm{H}}\mathbf{w}_{k,t}}{\mathbf{w}_{k,t}^{\mathrm{H}}\mathbf{Z}_{k,t}\mathbf{w}_{k,t}}, \tag{3}$$

where $\mathbf{Z}_{k,t} = \boldsymbol{\vartheta}_{k,t}\boldsymbol{\vartheta}_{k,t}^{\mathrm{H}} + \mathbf{z}_k\mathbf{z}_k^{\mathrm{H}}$ denotes the covariance matrix of the intra- and the inter-cell interference plus noise. For the case of a linear Minimum Mean-Square Error (MMSE) receiver, $\mathbf{w}_{k,t}$ is calculated as:

$$\mathbf{w}_{k,t} = v_{t,l}^{\mathrm{H}}H_{k,l}^{\mathrm{H}}(H_{k,l}v_{t,l}v_{t,l}^{\mathrm{H}}H_{k,l}^{\mathrm{H}} + \mathbb{E}\left[\mathbf{Z}_{k,t}\right])^{-1} \tag{4}$$

When a given mobile terminal is receiving more than one stream from its serving base station, it calculates a single effective SINR value starting from the SINR values associated to each stream. Specifically, the effective SINR, $\bar{\gamma}_k$, is obtained through an appropriate link-to-system model, that in our work is the Mutual Information Effective SINR Mapping (MIESM):

$$\bar{\gamma}_k = \beta I^{-1}\left(\frac{1}{N}\sum_{t \in \mathcal{T}_{l,k}} I\left(\frac{\gamma_{k,t}}{\beta}\right)\right), \tag{5}$$

where $\mathcal{T}_{l,k}$ is the set of streams sent to the k-th mobile terminal, N is the number of streams belonging to $\mathcal{T}_{l,k}$, $I(\cdot)$ is the mutual information function, and β is a tuning parameter [38].

4. Overview of evaluated technologies

The technologies evaluated in this work are presented in the following sections: Sec 4.1 illustrates the baseline LTE-A technology; Sec. 4.2 describes our implementation of mMIMO (a candidate technology for the 5G); and Sec. 4.3 explains its extension with the coordinated beamforming scheme (which is also a candidate technology for the 5G).

4.1. Baseline technology

In LTE, downlink transmissions can be driven according to many different Transmission Modes (TMs), which relate to different MIMO configurations [39]. While simpler configurations like Single-Input Single-Output (SISO) were also included to permit lower costs for initial deployments, the use of MIMO techniques was envisioned right from the beginning, to allow a high throughput. This work adopts Transmission Mode 9 (TM9) as the baseline technology. Introduced in Release 10, it allows up to 8x8 MIMO setups with spatial multiplexing and up to 8 layers.

An important element for the performance of TM9 is the CSI provided by the mobile terminal, which is used for precoding purposes. LTE adopts a codebook-based approach. For each configuration of TX antennas and for each transmission rank, there is a codebook of possible precoding matrices, which are uniquely identified by their indices [40]. The size of the codebooks depends on the number M of TX antennas. For $M = 2$, there are up to 4 possible precoding matrices (2-bit index). For $M = 4$, there can be up to 16 (4-bit index). For $M = 8$, up to 256 precoding matrices can be available (8-bit index). In all cases, the precoding codebook also depends on the reported Rank Indicator (RI), e.g. for $M = 2$ there is a rank-1 codebook and a rank-2 codebook. Moreover, the codebook for $M = 8$ is different from the others, because it is designed as a dual-index codebook. In fact, each precoding matrix $\mathbf{V}_l$ is the product of two matrices $\mathbf{V}_{l,1}$ and $\mathbf{V}_{l,2}$ extracted from two separate 4-bit codebooks [41]. Thus, the 8-bit index of $\mathbf{V}_l$ is simply the concatenation of the two indices of $\mathbf{V}_{l,1}$ and $\mathbf{V}_{l,2}$. $\mathbf{V}_{l,1}$

is intended to match the wideband and long-term statistics of the channel and can be reported less often, while $\mathbf{V}_{l,2}$ captures the short-term phase variations and is reported more often.

When receiving data, the mobile terminal acquires the channel matrix $\mathbf{H}_{k,l}$ via downlink training signals. This happens also when it needs to report the CSI, but it is not scheduled for reception. In either case, all the possible precoding matrices and all the possible rank values are tested against the channel matrix to find the best matching combination, i.e. the one which maximizes the expected throughput [42][43]. The index of the preferred matrix is then fed back to the base station, along with other feedback information, e.g., RI and Channel Quality Indicators (CQIs).

The precoding matrix indicated by the mobile terminal can be directly used at the base station for the next transmission. However, with TM9, the base station is not limited to use elements from the codebooks, but can use any other precoding matrix based on additional information (e.g., angle of arrival estimation).

4.2. Massive MIMO and JSDM

mMIMO is at the heart of the 3GPP standardization of the New Radio interface for the 5G [44]. Working below 6 GHz, it allows mobile operators to reuse existing sites in urban macro scenarios by upgrading the antenna arrays, as well as the baseband processing. This way, challenges for acquiring new sites for small cells can be minimized or delayed in the future.

At the physical layer, mMIMO addresses two main aspects, which typically hinder large throughput gains for conventional MIMO systems: (i) limited Signal-to-Noise Ratio (SNR) for coverage limited mobile terminals, especially inside of buildings, and (ii) limited rank and condition numbers of the MU-MIMO radio channel matrices, due to a low number of transmitting antennas. With mMIMO, a high rank ensures the simultaneous transmission of a high number of data streams per cell. Thus a cell might be able to serve ten to twenty instead of just around two mobile terminals.

Transmitted signal

| Second stage precoder (short-term) |

| First stage precoder (long-term) |

| Wireless channel |

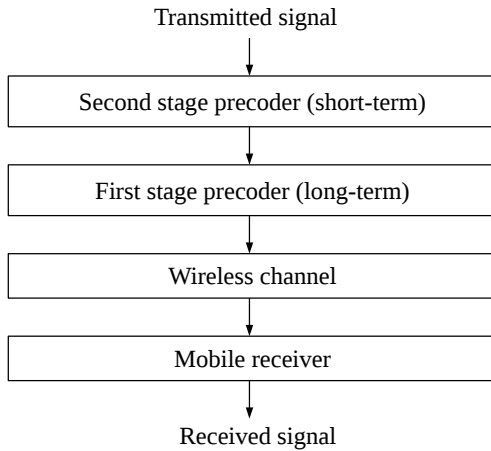| Mobile receiver |

Received signal

Figure 1: Block diagram of JSDM

There are some well known challenges related to mMIMO, like the channel estimation and the corresponding CSI feedback for a massive number of antenna elements when working in FDD mode [31]. A first, simple way forward to downscale the potentially very high number antennas to be considered, is the JSDM approach recently introduced by [12]. It is a two-stage beamforming/precoding scheme designed to handle inter-group interference based on second-order channel statistics on a long-term time scale and multi-user interference inside of a group based on short-term (instantaneous) CSI. Its block diagram is shown in Figure 1.

The first-stage precoding can take the form of a GoB, where a beamforming network is used to send independent signals in a number of fixed spatial directions, spanning the entire area of a cell sector. This choice comes from the observation that the covariance matrix for a uniform linear array is a Toeplitz matrix [45], which can be asymptotically approximated by a circulant matrix and then diagonalized with a DFT basis [46]. This arrangements provides a significant beamforming gain as well as a great reduction of the effective channel matrix size [47]. This, in turn, reduces the number of pilot sequences required in

15

the downlink, thus limiting the well-known pilot contamination issue. Further analysis indicates that the number of relevant channel components, i.e., those beams being received by a mobile terminal within a certain power window (for example 20 dB), will be only a subset of the total set of beams, which is the result of the spatial structuring due to the GoB beamforming. In other terms, the effective channel matrix is sparse (i.e. many elements can be approximated as zero), leading to a number of benefits like the further reduction of CSI reporting overhead or the limited processing power for calculation of the precoder matrices.

This concept is exploited in [37], resulting in a reporting scheme which reduces downlink training overhead to about 5%, while also preventing the pilot contamination problem. Such requirement is comparable with current LTE-A training overhead, and thus it is assumed to be the estimation and reporting overhead evaluated in this work.

To use a GoB configuration, the general precoding matrix $\mathbf{V}$ from Eq. (1), is split into two matrices by:

$$\mathbf{V}_l = \mathbf{B}_l \mathbf{C}_l, \tag{6}$$

with dimensions $\mathbf{B}_l \in \mathbb{C}^{M \times n}$ and $\mathbf{C}_l \in \mathbb{C}^{n \times T_l}$. The matrices $\mathbf{B}_l$ and $\mathbf{C}_l$ denote the GoB beamformer (first stage) and the RZF precoder (second stage), respectively. $n \in \mathbb{N}, T_l < n < M$ is the number of beams produced, and is a design parameter.

The contents of $\mathbf{B}_l$ depend, among other things, on the structure of the antenna array. For a uniformly spaced linear array, we can write:

$$\mathbf{B}_l = \begin{bmatrix} \mathbf{b}_{l,1}(M) & \mathbf{b}_{l,2}(M) & \dots & \mathbf{b}_{l,n}(M) \end{bmatrix}, \tag{7}$$

where $\mathbf{b}_{l,i}(k) \in \mathbb{C}^k$ is the precoder to produce the i-th beam using k antennas:

$$[\mathbf{b}_{l,i}(k)]_h = e^{j(h-1)\left(-\frac{2\pi}{\lambda} d \cos \theta_i\right)}, \tag{8}$$

where λ is the wavelength, d is the distance between antenna elements and θ_i is the angle between the array broadside direction and the desired horizontal direction of the i-th beam.

For a uniformly spaced $M_v \times M_h$ rectangular array, 3D beamforming becomes possible and the GoB precoding matrix becomes:

$$\mathbf{B}_l = \begin{bmatrix} \mathbf{b}'_{l,1,1}(M_h) & \mathbf{b}'_{l,1,2}(M_h) & \ldots & \mathbf{b}'_{l,1,n}(M_h) \\ \mathbf{b}'_{l,2,1}(M_h) & \mathbf{b}'_{l,2,2}(M_h) & \ldots & \mathbf{b}'_{l,2,n}(M_h) \\ \vdots & \vdots & \ddots & \vdots \\ \mathbf{b}'_{l,M_v,1}(M_h) & \mathbf{b}'_{l,M_v,2}(M_h) & \ldots & \mathbf{b}'_{l,M_v,n}(M_h) \end{bmatrix}, \tag{9}$$

where:

$$\mathbf{b}'_{l,q,i}(k) = \mathbf{b}_{l,i}(k)e^{j(q-1)\left(-\frac{2\pi}{\lambda}d\cos\phi_i\right)}, \tag{10}$$

and ϕ_i is the angle between the array broadside direction and the desired vertical direction of the i-th beam.

Finally, if the elements of the rectangular array are cross-polarized antenna pairs, then $\mathbf{B}_l$ can be simply rewritten as:

$$\mathbf{B}_l = \begin{bmatrix} \mathbf{B}_{l,1} & \mathbf{0} \\ \mathbf{0} & \mathbf{B}_{l,2} \end{bmatrix}, \tag{11}$$

where both $\mathbf{B}_{l,1}$ and $\mathbf{B}_{l,2}$ take the same form as $\mathbf{B}_l$ in Eq. 9.

Here we focus on carrier frequencies below 6 GHz, as they provide good overall coverage and all existing mobile networks already work at these frequencies. Note that, for below 6 GHz urban macro scenarios with multiple reflections and diffractions, serving ten or more users simultaneously lead to severe inter-user interference, so that simple beam selection would not be a good choice. Instead, typical precoders rely on Zero Forcing (ZF) or, in case of mobile terminals with limited SINR, on RZF precoders [36]. In this last case, the second-stage precoder $\mathbf{C}_l$ is calculated as:

$$\mathbf{C}_l = \mathbf{D}_l \mathbf{E}_l^{-\frac{1}{2}} \tag{12}$$

$$\mathbf{D}_l = [\mathbf{d}_{l,1}\mathbf{d}_{l,2}\ldots\mathbf{d}_{l,T_l}] = \mathbf{H}_l^H \mathbf{W}_l^H \left(\mathbf{W}_l \mathbf{H}_l \mathbf{H}_l^H \mathbf{W}_l^H + \sigma^2 \mathbf{I}_{T_l}\right)^{-1}, \tag{13}$$

where $\mathbf{H}_l$ is the compound channel matrix obtained by concatenating the channel matrices $\mathbf{H}_{k,l}$ of all the users being served, and likewise the receiver matrix

17

$\mathbf{W}_l$ is the concatenation of the (estimated) receive filters used at all the served receivers. $\mathbf{E}_l$ is a diagonal matrix used to enforce the total power constraint and improve the sum throughput, by assigning lower power to high-SINR users and high power to low-SINR users. It is calculated with the vector normalization method [48], which achieves a good balance between sum throughput and fairness among users:

$$[\mathbf{E}_l]_{i,i} = \mathbf{d}_{l,i}^H \mathbf{d}_{l,i} \tag{14}$$

4.3. Interference reduction with beam coordination

Motivated by the growing traffic demands described in Sec. 1, the densification of base stations in certain areas is expected to grow [49]. Such scenarios are often referred to as ultra-dense networks in literature [50][51]. In this context, the inter-cell interference management is required also with mMIMO. The idea is to use the first-stage GoB beamformer introduced in the previous Section for beam-coordination between base stations.

The JSDM was originally designed for a single mMIMO base station. However, the concept is extended to coordinate interference between multiple mMIMO base stations [52]. Preliminary results already presented in [14] promise significant performance gains. Still, the scenarios therein are simplified to only 2 and 3 base stations, which do not expose possible conflicts that arise in larger setups. This work extends that to a complete multi-site scenario.

In [14], the first stage precoders are selected out of a DFT matrix which enables easy implementation into existing system level environments. This concept combines the advantage of GoB to reduce dimensionality of the mMIMO channel and, at the same time, to provide spatial interference mitigation among interfering base stations.

In this work, an approach derived from [14] is adopted to reduce the average interference level. Three different GoB beamformers are defined which only cover a subset of the sector, instead of the entire sector as described in Sec. 4.2. Specifically, the sector's azimuth span of 120 degrees is split into three equal
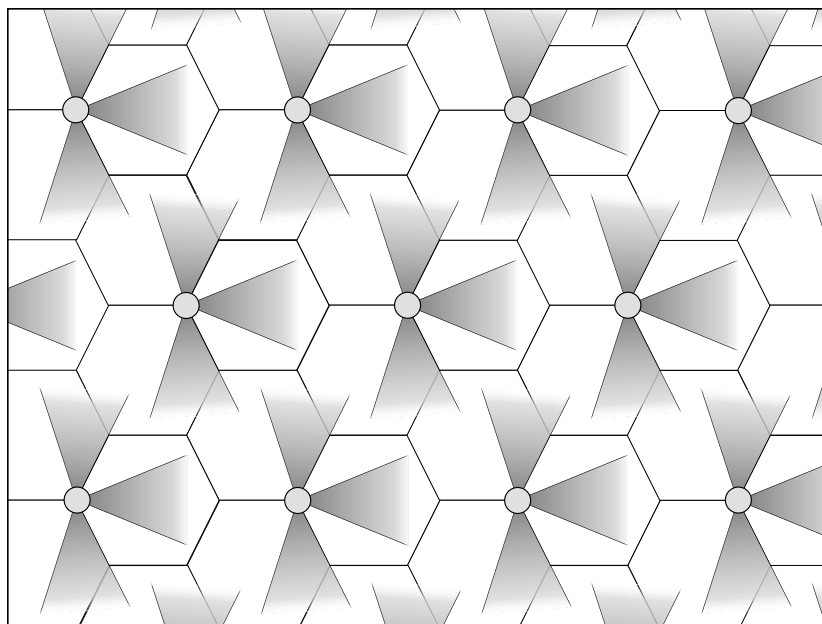
18

Figure 2: Example of coverage profile for coordinated beamforming

parts of 40 degrees each, with the beams of the first-stage precoder confined to one of the three sub-sectors. The three beamformers are changed frequently with a fixed or adaptive pattern. With traditionally sectorized base stations, this result could only be obtained by physically replacing the antenna arrays. On the contrary, with mMIMO this only requires a re-configuration of the first-stage precoder by the scheduler.

When considering the three sectors of one site, each sector uses a different beamformer and they are arranged so that in no case adjacent sub-sectors are served. Moreover, the same combination applied in one site is repeated verbatim on all the other sites. Accordingly, the use of a specific beamformer over multiple cells defines a *coverage profile*. One example profile is shown in Figure 2, the others are similar but rotated by ±120°. This configuration has a number of advantages:

- in the long term, all the sub-sectors can be served equally well;

- when looking at the complete multi-cell pattern, served sectors are never

19

facing each other directly at a close distance, thus reducing the interference $\mathbf{z}_k$ from (2) and raising the SINR;

- if the sequence of the beamformers to be used is known in advance, a User Equipment can go in a power saving state when his sub-sector is not being served;

- for inter-cell coordination, the only requirement is that the cells are time-synchronized and that they exchange the index of the beamformers configuration, which can only have three possible values;

- in sub-sectors which are not being served, pico/femto-cells (if present) can work with reduced interference levels.

The short term feedback for the second stage precoding is designed locally at each base station independently, based on the short term CSI, e.g., at base station l from the users connected to it.

5. Performance evaluation

The technologies presented in Sec. 4 were implemented in the open-source simulator LTE-Sim [21] and evaluated via computer simulations. Sec 5.1 describes the implementation details and parameters for each of the considered technologies, while Sec. 5.2 presents obtained results with relevant comments.

5.1. Implementation details and parameters

5.1.1. Common parameters

According to the Flexible Air iNTerfAce for Scalable service delivery wiThin wIreless Communication networks of the 5th Generation (FANTASTIC-5G) terminology, our study considers for two different scenarios: the first one is "50 Mbps Everywhere", including rural and suburban areas; the second one is "Dense Urban Society" for urban scenarios. Both scenarios include a standard layout of 19 sites (57 cells) placed on a hexagonal grid. However, results are

Table 3: Simulation parameters

Parameter	Value
Cellular deployment	hexagonal grid, 19 sites
ISD	200, 600, 1000 m
User density	100, 400, 2500 users/km^2
User distribution	uniform over simulation area
User speed	3 km/h
Carrier frequency	800MHz or 2 GHz
Operative bandwidth	100 MHz (5 x 20 MHZ)
Channel model	3GPP 3D channel model
Link-to-system mapping	MIESM
Shadowing std. dev.	10 dB
Indoor penetration loss	20 dB
Indoor/outdoor ratio	80%
Transmission power	46 dBm for each 20 MHz carrier
CQI reporting period	5 ms
Traffic model	Infinite buffer
Duration	10 s
Number of realizations	30

collected only for the center cell to obtain a realistic interference profile. The ISD is set to 200, 600, or 1000 m.

Mobile terminals are randomly distributed over the entire simulation area, with a uniform probability distribution. During the whole simulations, they move at a velocity of 3 km/h. According to the requirements of the considered use cases, the user density is set to 2500 users/km^2, 400 users/km^2, and 100 users/km^2 for the urban, suburban, and rural scenarios, respectively.

The total bandwidth is set to 100 MHz. This is achieved by using carrier aggregation on 5 component carriers of 20 MHz each. The center frequency is set to 2000 MHz for the urban/suburban case and 800 MHz for the rural case.

Regarding the channel model, we adopt the 3GPP 3D model, described in [53], for both large-scale path loss and small-scale fading. Shadow fading is modeled as a log-normal random variable with a standard deviation of 10 dB. The overall network embraces 80% of indoor users. They experience a penetration loss equal to 20 dB. The remaining 20% of users are outdoor and they do not experience any additional loss due to the penetration phenomenon.

The transmission power of the base station is set to 46 dBm for each 20 MHz carrier. The Modulation and Coding Scheme (MCS) and Transport Block Size (TBS) are selected according to procedures standardized in the LTE-A specifications, based on the predicted SINR at the receiver [39]. Specifically, the final user throughput is directly proportional to the selected TBS.

Mobile terminals send their feedback information (which can vary according to the adopted technology) with a periodicity of 5 ms. When receiving data at the physical layer, the SINRs of each sub-channel are calculated according to Eq. (3), which are then mapped to an effective SINR using the MIESM formula of Eq. (5). Finally, the probability of receiving a corrupted block, i.e. the Block Error Rate (BLER), is calculated according to pre-calculated SINR-BLER curves in an equivalent AWGN channel.

To look for the upper bound on the throughput performance, we choose an infinite-buffer traffic model at the application layer. Each simulation is repeated 30 times with a different initial seed, which affects random variables such as user

position and fast fading realizations. All the simulation parameters described so far are summarized in Table 3.

5.1.2. LTE-A TM9

The baseline LTE-A technology, considered as a term of comparison, uses a physical layer based on TM9 and a MIMO transmission scheme with the 8x8 configuration. This is a rather optimistic assumption for the present time, as mobile terminals with 8 antennas are still not seen in the consumer market, but this may change at some point and we decided to assume their future availability. Specifically, the antenna array at the base station is an Uniform Linear Array (ULA) with vertical polarization and $\lambda/2$ element spacing, while the mobile terminal has a cross-polarized array with $\lambda/2$ spacing as well.

The Single-User MIMO (SU-MIMO) mode is used, i.e. only one user is scheduled in a cell at any given time, with a round-robin criterion. Also, pre-coding is done according to the dual-index codebook defined for operation with 8 transmission antennas.

At the receiving side, the mobile terminal calculates the SINR using a linear MMSE receiver and send back feedback information: the CQI for link adapta-tion, and Precoding Matrix Indicator (PMI) plus RI for hints on the preferred MIMO processing at the base station. PMI and RI are calculated via an exten-sive search over all the possible combinations, and the one which maximizes the predicted throughput is selected. CQI is finally calculated with respect to the resulting expected SINR with the chosen PMI and RI.

5.1.3. mMIMO+JSDM

The antenna array used for mMIMO contains 16 elements in the horizontal direction and 8 elements in vertical direction, with $\lambda/2$ spacing in both direc-tions. Each element is actually a dual-polarized antenna, with ±45° orientations.

The GoB precoding creates 16 beams in the horizontal direction, with equally spaced boresight directions spanning the entire area of the cell (i.e. a 120° sector). The vertical dimension is exploited by giving different tilting angles to

even-numbered and odd-numbered beams. Each beam is created by both left and right slanted antennas. Thus, there are 32 beams in total.

On top of GoB, the RZF precoding is applied to map data streams to beams with appropriate weights and phases. In this case a MU-MIMO configuration is employed, where up to 8 devices can be scheduled on the same physical resources. This amounts to a total of 16 data streams, against the maximum theoretical 32. Because of how the RZF precoder works, using more than half of the possible streams reduces the available degrees of freedom and degrades the performance rapidly. The users to be served are selected with a multi-user version of the round-robin scheduler. Specifically, the scheduler selects a new set of users for each Transmission Time Interval (TTI), shifting over the list of registered users. When it reaches the end of the list, it just resumes from the beginning.

After the RZF, vector normalization as described in [48] is performed on the obtained precoding vectors, to partially compensate for the different path losses and provide a good compromise between total throughput and fairness.

Mobile terminals are equipped with two receive antennas in a cross-polarized configuration, and they are configured to receive two layers of spatially-multiplexed data. They use a linear MMSE receiver to evaluate the received SINR, which is then used for BLER estimation and CQI feedback. In this work, CQIs are calculated by using the same SINR-CQI mapping as in LTE-A.

Regarding the CSI reporting scheme, the proposed study initially assumes a perfect knowledge of the CSI at the base station side. In practice, in fact, a high accuracy can be achieved with reasonable uplink data rates, by reporting only relevant beams/taps as shown in [37] or [35]. Then, to provide a further insight, the conducted study also evaluated the impact that a reduction of CSI feedbacks has on the overall system performance.

5.1.4. Coordinated beamforming

For the coordinated beamforming scheme, three different profiles are used. They are obtained by dividing the area of a sector into three sub-sectors in the

angular domain, as already described in Section 4.3.

For the scheduling, it is important to only consider users which are in sub-sectors with good coverage. Therefore, users have to observe the signal quality over all the coverage profiles and indicate the preferred one to the base station.

All the other parameters presented for mMIMO also apply here.

### 5.2. Simulation results

5.2.1. Impact on the channel quality

The performance of the proposed technologies is firstly evaluated in terms of channel quality experienced by mobile terminals. Such a performance index is expressed by means of the post-detection SINR, calculated accordingly to Eq. (3). In order to have a first look of the SINR within a cell, Figure 3 reports the SINR map measured in a scenario with ISD=500 m and user density equal to 100 users/km^2. Note that even if a multi-cell environment is simulated, reported results only show what is registered in the central cell.

Figure 3a shows the spatial SINR distribution obtained with the baseline LTE-A technology. Here, the main lobes of the three sectors are clearly visible, as well as the large gaps at the sector boundaries with low SINR ($\gamma < 5\,\mathrm{dB}$). The SINR ranges from 10-15 dB in the main lobes, down to 0 at the cell edges.

Figure 3b represents the same information for mMIMO with GoB. In this case, the SINR is much higher due to the high directivity gain, while the weak inter-sector areas are drastically reduced. This clearly reflects a large improvement of the perceived channel quality, which in turn permits greater throughputs.

Figure 3c, Figure 3d, and Figure 3e show the SINR distribution for the three coverage profiles of the coordinated beamforming, while Figure 3f picks the maximum of the three values for each point. This configuration provides a further increment of the SINR, due to the reduction of the interfering power, with a more uniform coverage as well.
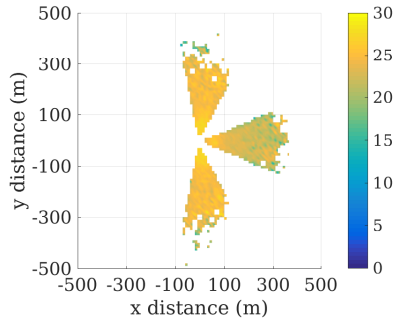
A more comprehensive analysis is reported in Figure 4, Figure 5, and Figure 6, which show the Cumulative Density Function (CDF) of the post-detection
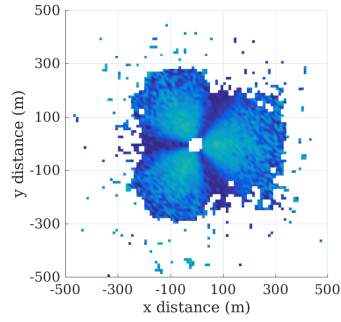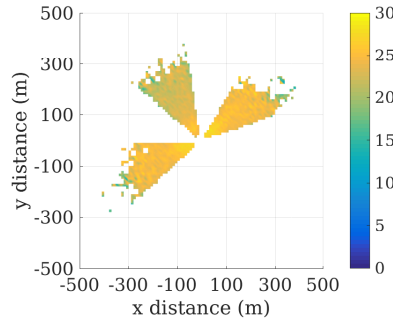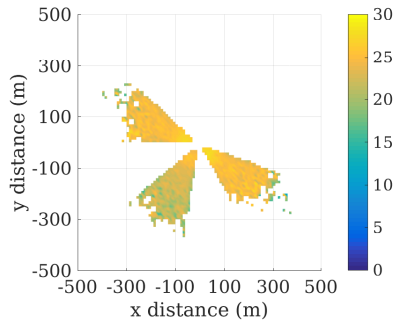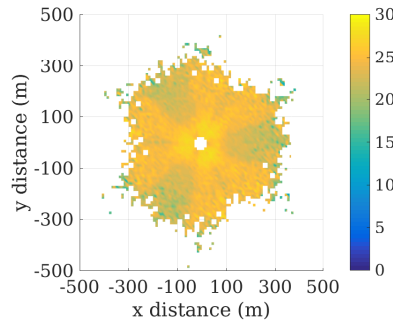
(a) LTE-A
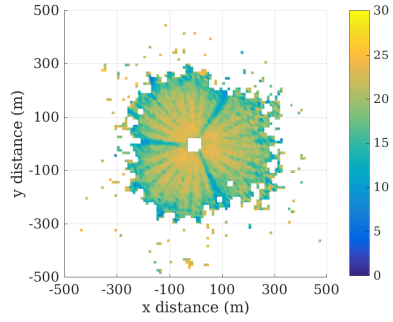
(b) mMIMO

(c) mMIMO with coordinated beamforming, profile 0

(d) mMIMO with coordinated beamforming, profile 1

(e) mMIMO with coordinated beamforming, profile 2

(f) mMIMO with coordinated beamforming, maximum values for all the profiles

Figure 3: Example of the SINR map for LTE-A, mMIMO, and the coordinated beamforming, obtained in a scenario with an ISD of 500 m and user density equal to 100 users/km^2.
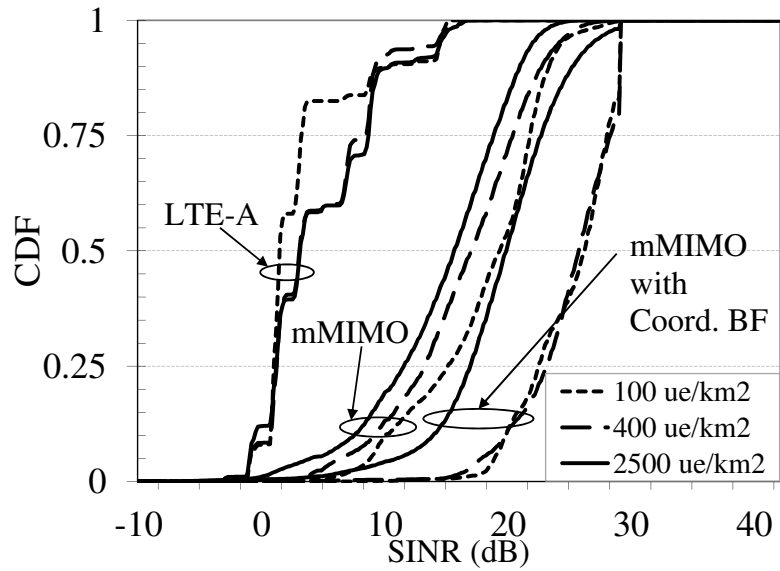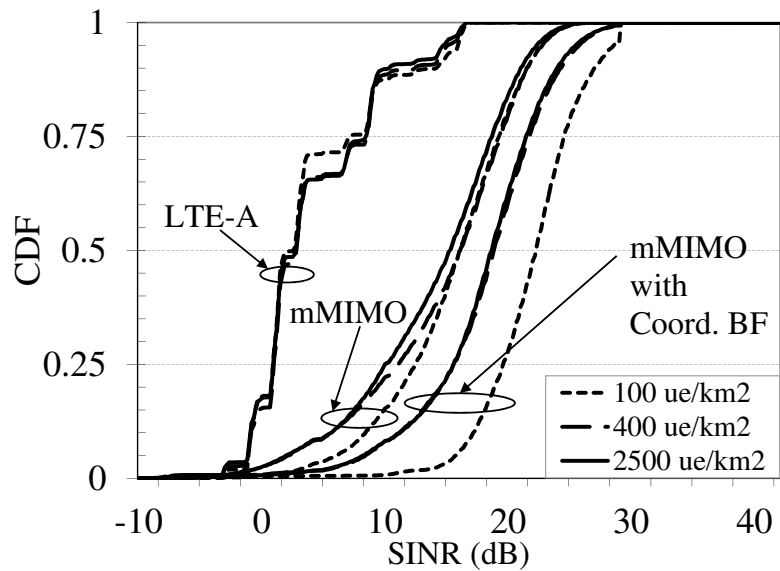
Figure 4: Cumulative distribution function of SINR (ISD = 200 m)

Figure 5: Cumulative distribution function of SINR (ISD = 600 m)
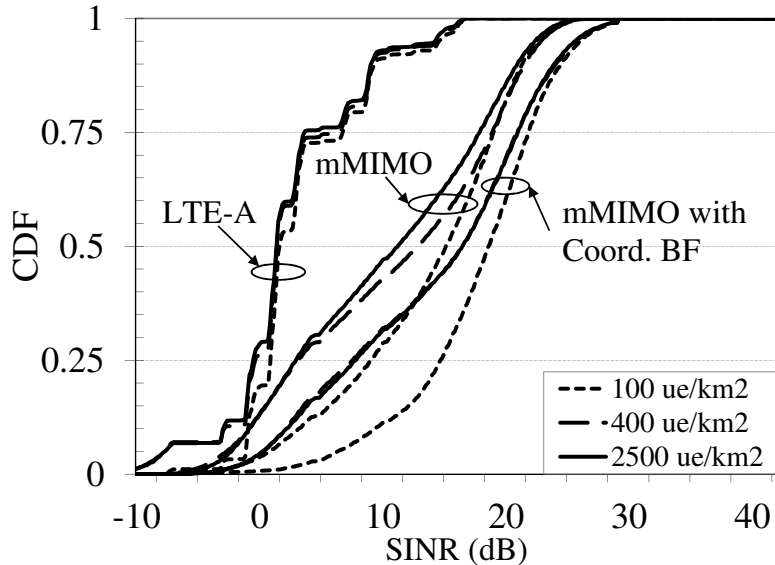
27

Figure 6: Cumulative distribution function of SINR (ISD = 1000 m)

SINR for all the combinations of ISD and user density. In accordance with previous comments, LTE-A is always surpassed by mMIMO, which in turn is surpassed by mMIMO with coordinated beamforming. Note that the LTE-A curves are not smooth as an effect of the dynamic rank adaptation.

For all the technologies, it is possible to observe that an increment in the ISD produces a shift towards lower SINRs. This effect is expected, as it is due the increment of the average path loss. On the contrary, the user density has a different impact on LTE-A compared to the proposed 5G solutions. With mMIMO and mMIMO with coordinated beamforming, for instance, a higher user density results in a higher average number of co-scheduled users. Thus, the power transmitted to each user is lower and the SINR is reduced as well. On the other hand, LTE-A has very little variation on the user density. The only exception is the curve for ISD of 200 m and density of 100 users/km^2. This is probably due to statistical fluctuations, because it is a scenario with a very low number of users per sector.

5.2.2. KPIs investigation

Figure 7, Figure 8, and Figure 9 report the results for the user experienced data rate, defined as the average data rate achieved by each user over an entire simulation run. It is reported for all the evaluated technologies, all ISDs, and all density values. We recall that the target value is 50 Mbps per user. The LTE-A technology is able to meet the required value in only three instances, that is, when the number of users is relatively low compared to the number of base stations: with an ISD of 200 m and $100/400$ users/km^2, or with an ISD of 600 m and 100 users/km^2. These can be considered as oversized cases, therefore they are of limited practical interest. In the other (more challenging) scenarios, instead, LTE-A is not able to guarantee a sufficient data rate. On the other hand, mMIMO and mMIMO with coordinated beamforming can reach nearly one order of magnitude of gain. Specifically, they provide more than 100 Mbps (i.e. twice the required value) also in these three scenarios, which have an higher ratio between users and base stations: 1000 m ISD $+$ 100 users/km^2, 600 m ISD $+$ 400 users/km^2, and 200 m ISD $+$ 2500 users/km^2. We can call these deployments "balanced scenarios", as the number of users per cell is in a reasonable range (i.e., from 30 to 50). Finally, the remaining three combinations (1000 m ISD $+$ 400 users/km^2, 600 m ISD $+$ 2500 users/km^2, and 1000 m ISD $+$ 2500 users/km^2) are the undersized cases, because there are so many mobile terminals in each cell that they cannot reach the required data rate.

It is interesting to note that, in the oversized cases only, coordinated beamforming performs worse than mMIMO, despite the average SINR being higher. This happens because for this technology the number of users available for scheduling is further reduced by the sub-sectorization of the cells, and the full capacity can not be exploited. In all the other cases, coordinated beamforming provides a gain of around 20% with respect to mMIMO.

To provide a further insight, Figure 10, Figure 11, and Figure 12 show the CDF of the user experienced data rate for the three "balanced scenarios". They confirm that most of the transmissions performed with the newer schemes (i.e.,
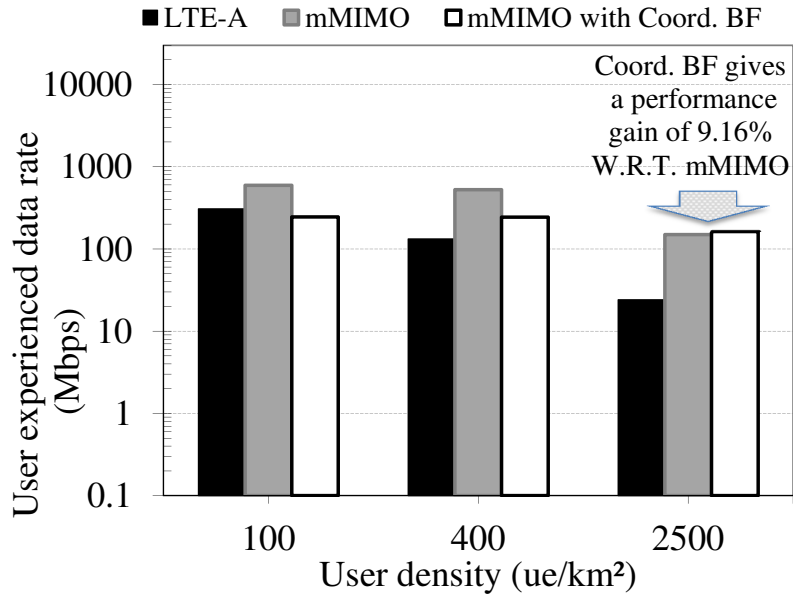
29

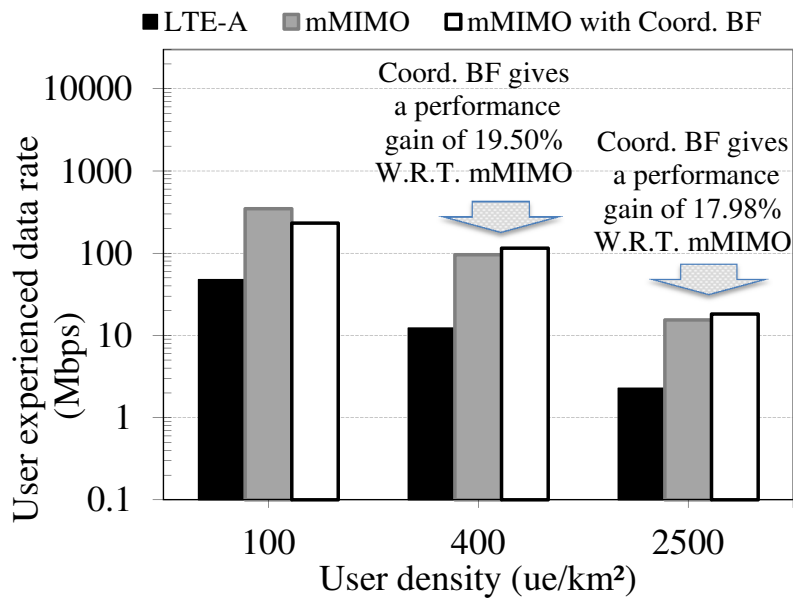Figure 7: User experienced data rate (ISD = 200 m)

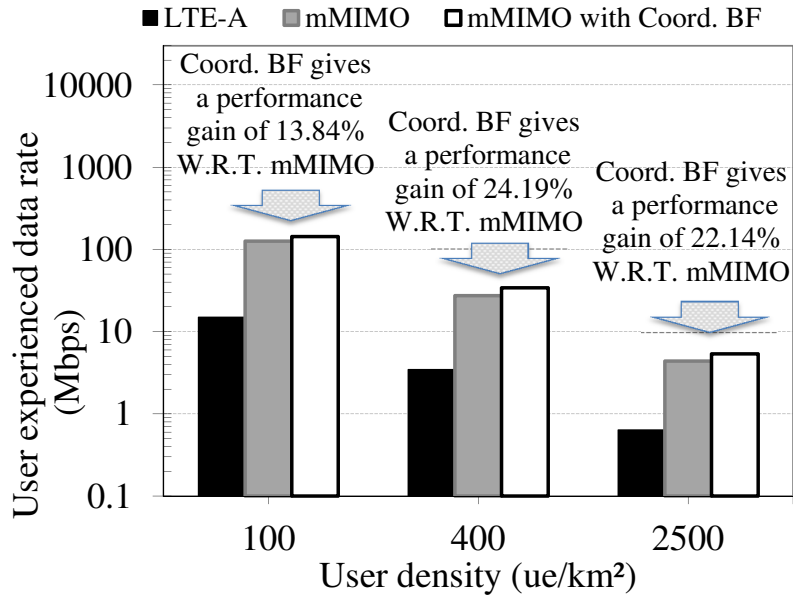Figure 8: User experienced data rate (ISD = 600 m)

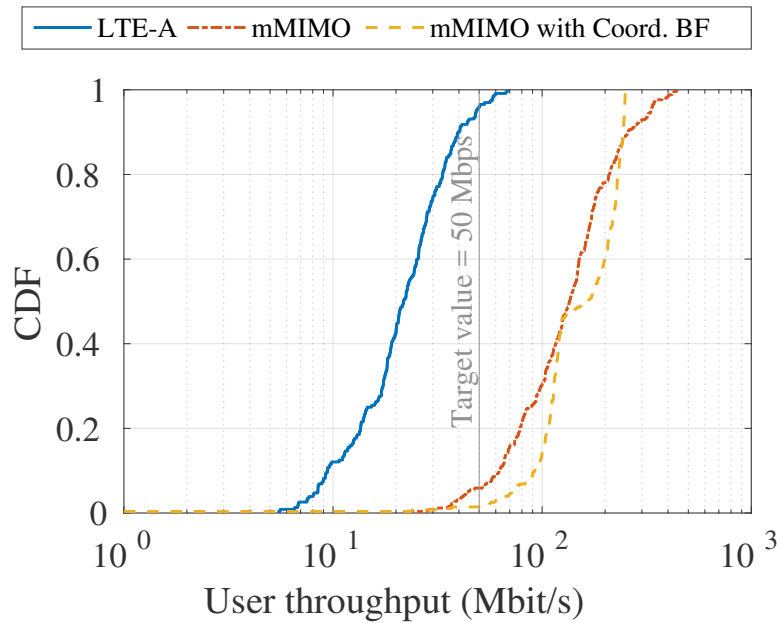Figure 9: User experienced data rate (ISD = 1000 m)

Figure 10: Cumulative distribution function of user throughput (ISD = 200 m)
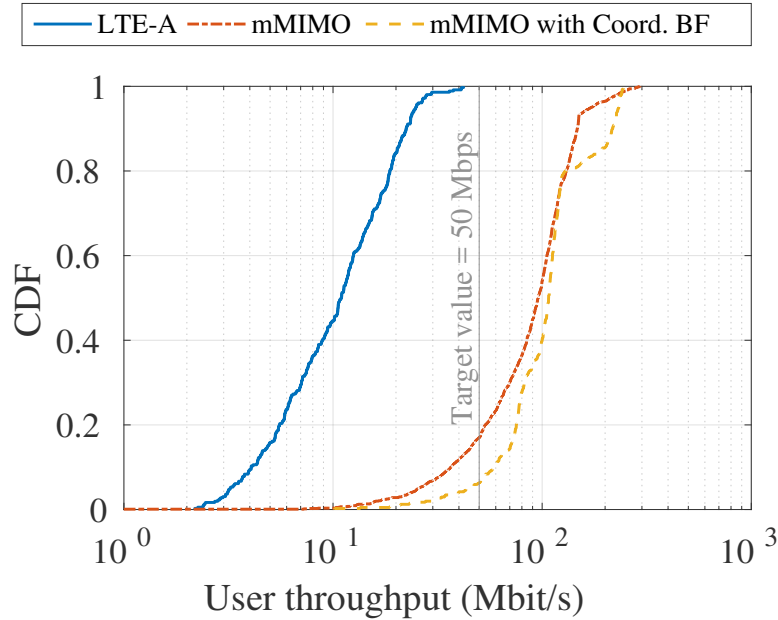
Figure 11: Cumulative distribution function of user throughput (ISD = 600 m)

mMIMO and mMIMO with coordinated beamforming) can achieve a throughput much higher than the target value. Moreover, they show that the gain provided by the coordinated beamforming scheme is quite consistent across the entire curve, and it is effective at improving the 95 %-ile of the throughput.

Table 4 shows the measured traffic density, defined as the ratio of aggregate traffic in a given area (e.g., a cell) over the size of such area. In this case the target values (obtained from the requirements of FANTASTIC-5G[22]) are different for each scenario: 5, 20, and 125 Gbps/km^2 for user density of 100, 400 , and 2500 users/km^2, respectively. With respect to these target values, the behaviour of the traffic density is very similar to the user experienced data rate: LTE-A meets the requirements only in the oversized cases, while mMIMO and mMIMO with coordinated beamforming provide good results also in the balanced cases (but not in the undersized cases). Again, coordinated beamforming performs worse in the oversized cases, but provides around 20% gain in all the
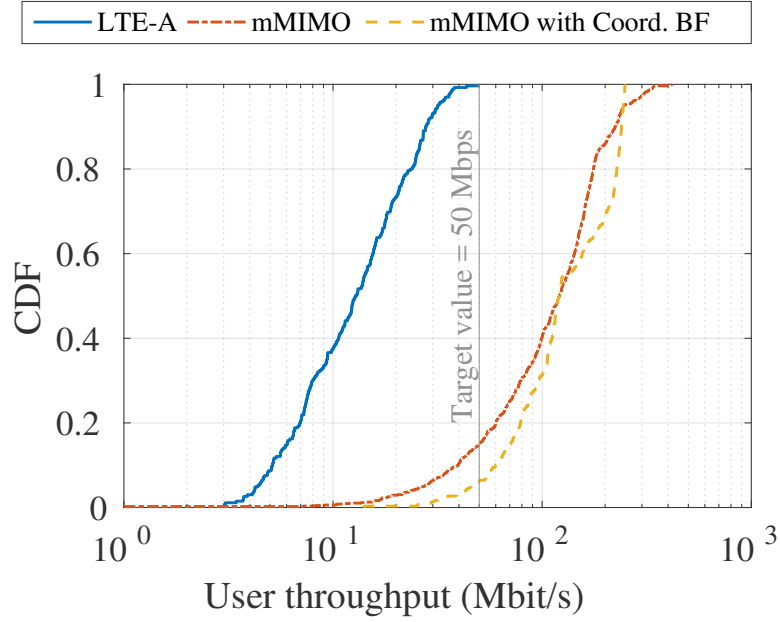
Figure 12: Cumulative distribution function of user throughput (ISD = 1000 m)

Table 4: Traffic density [Gbps/km^2]

			Inter-site distance (Km)		
			0.2	0.6	1
	100	LTE-A	23.9	4.09	1.38
		mMIMO	65.0	36.2	12.4
		mMIMO with Coord. BF	21.2	20.8	14.7
User density (users/km^2)	400	LTE-A	39.0	4.24	1.18
		mMIMO	205	37.0	10.8
		mMIMO with Coord. BF	78.1	44.7	13.0
	2500	LTE-A	48.4	4.95	1.42
		mMIMO	330	35.2	10.1
		mMIMO with Coord. BF	393	44.9	13.1

Table 5: Cell throughput [Gbps]

			Inter-site distance (Km)		
			0.2	0.6	1
User density (users/km²)	100	LTE-A	0.276	0.425	0.397
		mMIMO	0.750	3.76	3.59
		mMIMO with Coord. BF	0.245	2.16	4.24
	400	LTE-A	0.450	0.441	0.341
		mMIMO	2.36	3.85	3.11
		mMIMO with Coord. BF	0.902	4.65	3.76
	2500	LTE-A	0.560	0.515	0.409
		mMIMO	3.81	3.66	2.90
		mMIMO with Coord. BF	4.54	4.66	3.78

other situations.

It is interesting to note that the increment of the user density results in a higher area throughput, but only when oversized and balanced scenarios are considered. On the contrary, when going from balanced to undersized scenarios, the traffic density is fairly stable, meaning that the full potential of the network is already being used.

This is also confirmed by Table 5, which reports the total throughput of one cell, but without normalization with respect to the area. In this case it is even more apparent that balanced/undersized scenarios all reach similar results, corresponding to the practical limit of the system.

5.2.3. Additional investigation on the CSI acquisition

As already mentioned, the two-stage precoding structure natively reduces the CSI overhead, as the number of pilot signals to transmit and feed back is equal to the number of beams, rather then the number of physical antennas. Moreover, additional savings can be obtained by only reporting the most relevant beams and discarding those with very low received power. This approach is

usually implemented by comparing the quality of beams agaonst the strongest one through a given threshold. For instance, adopting a threshold of 25 dB means that any beam that is more than 25 dB weaker than the stronger beam is completely neglected. Of course, this would cause an additional inter-user interference, because the effect of such beams is not considered anymore by the RZF precoder.

In this section, we investigate the effect of different threshold values for CSI reporting on the user throughput. The results are shown in Figure 13, for the three balanced scenarios identified in Section 5.2.2 and for the JSDM + coordinated beamforming scheme only. An higher threshold value means that more beams are included in the CSI report and the precoding is more precise, while lower values reduce the set of reported beams but also incur more interference and lower SINRs. The results are expressed as a percentage of the throughput of the ideal case, i.e. the throughput is 100% when all the beams are reported, and decreases as more beams are excluded. The overall effect is similar for the three scenarios: threshold values of 35 dB or higher give almost as much throughput as the ideal case, and with 30 dB more than 90% of the throughput is still maintained. Instead, with lower values of 25 dB and 20 dB, the throughput degrades more rapidly, thus they should probably be avoided, although the actual throughput is still within the target requirements stated in Section 1. In general, 30 dB appears to be the most reasonable compromise between CSI precision and feedback reduction.

6. Conclusion

In this work, we evaluate some candidate 5G technologies with the aim to provide wideband Internet connectivity over cellular networks, in the context of macro-cellular deployments with different ISDs. The evaluation is carried out using computer simulations, comparing the proposed technologies against a baseline LTE-A deployment. Obtained results show that the LTE-A system is not able to meet the requirements envisioned for the future connected society
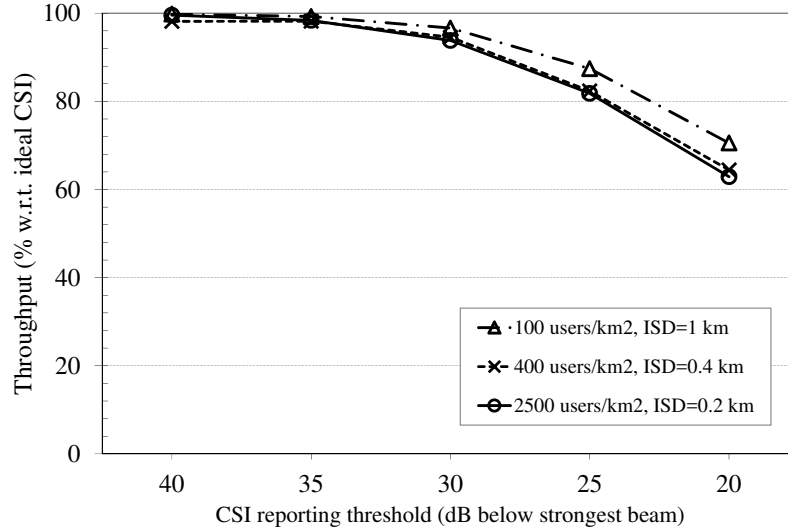
Figure 13: Effect of CSI acquisition threshold

in the aforementioned scenarios. On the contrary, using mMIMO as the transmission technology permits a large increment of the achieved throughput (from around 550% to 850%) under reasonable operating conditions. We also evaluated a coordinated beamforming technique to reduce the interference, which provides an additional gain of 10% to 20%. Future developments of this work may include different antenna array structures and parameters, Coordinated Multi-Point transmission, and heterogeneous network deployments with small cells.

Acknowledgments

References

[1] Cisco, Cisco Visual Networking Index: Global Mobile Data Traffic Forecast Update, 2015-2020, Cisco Visual Networking Index: Global Mobile Data Traffic Forecast 1 (2016) 1–39.

[2] N. Alliance, 5G White Paper, Next Generation Mobile Networks, White paper.

[3] J. G. Andrews, S. Buzzi, W. Choi, S. V. Hanly, A. Lozano, A. C. Soong, J. C. Zhang, What will 5G be?, IEEE Journal on selected areas in communications 32 (6) (2014) 1065–1082.

[4] Y. Yifei, Z. Longming, Application scenarios and enabling technologies of 5G, China Communications 11 (11) (2014) 69–79.

[5] T. L. Marzetta, Noncooperative cellular wireless with unlimited numbers of base station antennas, IEEE Transactions on Wireless Communications 9 (11) (2010) 3590–3600.

[6] L. Lu, G. Y. Li, A. L. Swindlehurst, A. Ashikhmin, R. Zhang, An overview of massive MIMO: Benefits and challenges, IEEE Journal of Selected Topics in Signal Processing 8 (5) (2014) 742–758.

[7] E. G. Larsson, O. Edfors, F. Tufvesson, T. L. Marzetta, Massive MIMO for next generation wireless systems, IEEE Communications Magazine 52 (2) (2014) 186–195.

[8] Z. Jiang, A. F. Molisch, G. Caire, Z. Niu, Achievable rates of FDD massive MIMO systems with spatial channel correlation, IEEE Transactions on Wireless Communications 14 (5) (2015) 2868–2882.

[9] X. Rao, V. K. Lau, Distributed compressive CSIT estimation and feedback for FDD multi-user massive MIMO systems, IEEE Transactions on Signal Processing 62 (12) (2014) 3261–3271.

[10] M. S. Sim, J. Park, C.-B. Chae, R. W. Heath, Compressed channel feedback for correlated massive MIMO systems, Journal of Communications and Networks 18 (1) (2016) 95–104.

[11] J. Choi, D. J. Love, P. Bidigare, Downlink training techniques for FDD massive MIMO systems: Open-loop and closed-loop training with memory, IEEE Journal of Selected Topics in Signal Processing 8 (5) (2014) 802–814.

[12] A. Adhikary, J. Nam, J.-Y. Ahn, G. Caire, Joint Spatial Division and Multiplexing: The Large-Scale Array Regime, Information Theory, IEEE Transactions on 59 (10) (2013) 6441–6463. `doi:10.1109/TIT.2013.2269476`.

[13] F. Schaich, B. Sayrac, S. Elayoubi, I.-P. Belikaidis, M. Caretti, A. Georgakopoulos, X. Gong, E. Kosmatos, H. Lin, P. Demestichas, et al., FANTASTIC-5G: flexible air interface for scalable service delivery within wireless communication networks of the 5th generation, Transactions on Emerging Telecommunications Technologies 27 (9) (2016) 1216–1224.

[14] M. Kurras, L. Thiele, G. Caire, Multi-stage beamforming for interference coordination in massive MIMO networks, in: 2015 49th Asilomar Conference on Signals, Systems and Computers, 2015, pp. 700–703. `doi: 10.1109/ACSSC.2015.7421223`.

[15] F. W. Vook, A. Ghosh, T. A. Thomas, MIMO and beamforming solutions for 5G technology, in: Microwave Symposium (IMS), 2014 IEEE MTT-S International, IEEE, 2014, pp. 1–4.

[16] J. Nam, J.-Y. Ahn, A. Adhikary, G. Caire, Joint spatial division and multiplexing: Realizing massive MIMO gains with limited channel state information, in: Information Sciences and Systems (CISS), 2012 46th Annual Conference on, IEEE, 2012, pp. 1–6.

[17] B. L. Ng, Y. Kim, J. Lee, Y. Li, Y.-H. Nam, J. Zhang, K. Sayana, Fulfilling the promise of massive MIMO with 2D active antenna array, in: Globecom Workshops (GC Wkshps), 2012 IEEE, IEEE, 2012, pp. 691–696.

[18] Y. Kim, H. Ji, H. Lee, J. Lee, B. L. Ng, J. Zhang, Evolution beyond LTE-advanced with Full Dimension MIMO, in: Communications Workshops (ICC), 2013 IEEE International Conference on, IEEE, 2013, pp. 111–115.

[19] 3GPP, Study on Elevation Beamforming/Full-Dimension (FD) MIMO for LTE, TR 36.897, 3rd Generation Partnership Project (3GPP) (2015).

[20] ZTE, R1-1715253 Calibration results for Phase 2 NR MIMO system level calibration, in: V3GPP TSG RAN WG1 Meeting #90, 3GPP, 2017.

[21] G. Piro, L. A. Grieco, G. Boggia, F. Capozzi, P. Camarda, Simulating LTE cellular systems: An open-source framework, IEEE transactions on vehicular technology 60 (2) (2011) 498–513.

[22] FANTASTIC5G, Deliverable D2.1 Air interface framework and specification of system level simulations, Tech. Rep. D2.1, Call: H2020-ICT-2014-2, Project reference: 671660, Flexible Air iNTerfAce for Scalable service delivery wiThin wIreless Communication networks of the 5th Generation (FANTASTIC-5G) (May 2016).

[23] J. Choi, J. Mo, R. W. Heath, Near maximum-likelihood detector and channel estimator for uplink multiuser massive MIMO systems with one-bit ADCs, IEEE Transactions on Communications 64 (5) (2016) 2005–2018.

[24] J. Vieira, F. Rusek, F. Tufvesson, Reciprocity calibration methods for massive MIMO based on antenna coupling, in: Global Communications Conference (GLOBECOM), 2014 IEEE, IEEE, 2014, pp. 3708–3712.

[25] K. Zheng, S. Ou, X. Yin, Massive MIMO channel models: A survey, International Journal of Antennas and Propagation 2014.

[26] J. Jose, A. Ashikhmin, T. L. Marzetta, S. Vishwanath, Pilot contamination and precoding in multi-cell TDD systems, IEEE Transactions on Wireless Communications 10 (8) (2011) 2640–2651.

[27] O. Elijah, C. Y. Leow, T. A. Rahman, S. Nunoo, S. Z. Iliya, A comprehensive survey of pilot contamination in massive MIMO-5G system, IEEE Communications Surveys & Tutorials 18 (2) (2016) 905–923.

[28] A. Ashikhmin, T. Marzetta, Pilot contamination precoding in multi-cell large scale antenna systems, in: Proc. of IEEE International Symposium on Information Theory Proceedings (ISIT), IEEE, 2012, pp. 1137–1141.

[29] F. Fernandes, A. Ashikhmin, T. L. Marzetta, Inter-cell interference in non-cooperative TDD large scale antenna systems, IEEE Journal on Selected Areas in Communications 31 (2) (2013) 192–201.

[30] S.-C. Lin, H. Narasimhan, Towards Software-Defined Massive MIMO for 5G&B Spectral-Efficient Networks, in: Proc. of IEEE ICC, IEEE, 2018.

[31] E. Björnson, E. G. Larsson, T. L. Marzetta, Massive MIMO: Ten myths and one critical question, IEEE Communications Magazine 54 (2) (2016) 114–123.

[32] D. Gesbert, S. Hanly, H. Huang, S. S. Shitz, O. Simeone, W. Yu, Multi-cell MIMO cooperative networks: A new look at interference, IEEE Journal on Selected Areas in Communications 28 (9) (2010) 1380–1408.

[33] J. Choi, Z. Chance, D. J. Love, U. Madhow, Noncoherent trellis coded quantization: A practical limited feedback technique for massive MIMO systems, IEEE Transactions on Communications 61 (12) (2013) 5016–5029.

[34] W. Zirwas, L. Thiele, M. Kurras, G. Wunder, Flexible 5G below 6GHz mobile broadband radio air interface, in: Vehicular Technology Conference (VTC Spring), 2016 IEEE 83rd, IEEE, 2016, pp. 1–5.

[35] M. Kurras, S. Jaeckel, L. Thiele, V. Braun, CSI Compression and Feedback for Network MIMO, in: Vehicular Technology Conference (VTC Spring), 2015 IEEE 81st, IEEE, 2015, pp. 1–5.

[36] C. B. Peel, B. M. Hochwald, A. L. Swindlehurst, A vector-perturbation technique for near-capacity multiantenna multiuser communication-part I: channel inversion and regularization, IEEE Transactions on Communications 53 (1) (2005) 195–202.

[37] W. Zirwas, M. B. Amin, M. Sternad, Coded CSI Reference Signals for 5G-Exploiting Sparsity of FDD Massive MIMO Radio Channels, in: Proc. of 20th International ITG Workshop on Smart Antennas (WSA 2016), VDE, 2016, pp. 1–8.

[38] X. He, K. Niu, Z. He, J. Lin, Link layer abstraction in MIMO-OFDM system, in: Proc. of International Workshop on Cross Layer Design, IEEE, 2007, pp. 41–44.

[39] 3GPP, Evolved Universal Terrestrial Radio Access (E-UTRA); Physical layer procedures, TS 36.213, 3rd Generation Partnership Project (3GPP) (Sep. 2016).

[40] J. Lee, J.-K. Han, J. C. Zhang, MIMO technologies in 3GPP LTE and LTE-advanced, EURASIP Journal on Wireless Communications and Networking 2009 (1) (2009) 302092.

[41] T. Shuang, T. Koivisto, H.-L. Maattanen, K. Pietikainen, T. Roman, M. Enescu, Design and evaluation of LTE-Advanced double codebook, in: Vehicular Technology Conference (VTC Spring), 2011 IEEE 73rd, IEEE, 2011, pp. 1–5.

[42] Y.-H. Lin, Y.-H. Chen, C.-Y. Chu, C.-Z. Zhan, A.-Y. Wu, Dual-mode low-complexity codebook searching algorithm and VLSI architecture for LTE/LTE-advanced systems, IEEE Transactions on Signal Processing 61 (14) (2013) 3545–3562.

[43] S. Schwarz, M. Wrulich, M. Rupp, Mutual information based calculation of the precoding matrix indicator for 3GPP UMTS/LTE, in: Smart Antennas (WSA), 2010 International ITG Workshop on, IEEE, 2010, pp. 52–58.

[44] M. Shafi, A. F. Molisch, P. J. Smith, T. Haustein, P. Zhu, P. De Silva, F. Tufvesson, A. Benjebbour, G. Wunder, 5G: A Tutorial Overview of Standards, Trials, Challenges, Deployment, and Practice, IEEE Journal on Selected Areas in Communications 35 (6) (2017) 1201–1221.

[45] D. Neumann, M. Joham, L. Weiland, W. Utschick, Low-complexity computation of lmmse channel estimates in massive mimo, in: Smart Antennas (WSA 2015); Proceedings of the 19th International ITG Workshop on, VDE, 2015, pp. 1–6.

[46] R. M. Gray, et al., Toeplitz and circulant matrices: A review, Foundations and Trends® in Communications and Information Theory 2 (3) (2006) 155–239.

[47] J. Nam, A. Adhikary, J.-Y. Ahn, G. Caire, Joint spatial division and multiplexing: Opportunistic beamforming, user grouping and simplified downlink scheduling, IEEE Journal of Selected Topics in Signal Processing 8 (5) (2014) 876–890.

[48] Y.-G. Lim, C.-B. Chae, G. Caire, Performance analysis of massive MIMO for cell-boundary users, IEEE Transactions on Wireless Communications 14 (12) (2015) 6827–6842.

[49] N. Bhushan, J. Li, D. Malladi, R. Gilmore, D. Brenner, A. Damnjanovic, R. Sukhavasi, C. Patel, S. Geirhofer, Network densification: the dominant theme for wireless evolution into 5G, Communications Magazine, IEEE 52 (2) (2014) 82–89. `doi:10.1109/MCOM.2014.6736747`.

[50] M. Polignano, P. Mogensen, P. Fotiadis, L. Chavarria, I. Viering, P. Zanier, The Inter-Cell Interference Dilemma in Dense Outdoor Small Cell Deployment, in: Vehicular Technology Conference (VTC Spring), 2014 IEEE 79th, 2014, pp. 1–5. `doi:10.1109/VTCSpring.2014.7023122`.

[51] V. Jungnickel, K. Manolakis, W. Zirwas, B. Panzner, V. Braun, M. Lossow, M. Sternad, R. Apelfröjd, T. Svensson, The role of small cells, coordinated

multipoint, and massive MIMO in 5G, Communications Magazine, IEEE 52 (5) (2014) 44–51. `doi:10.1109/MCOM.2014.6815892`.

[52] M. Kurras, L. Thiele, G. Caire, Interference Mitigation and Multiuser Multiplexing with Beam-Steering Antennas, in: WSA 2015; 19th International ITG Workshop on Smart Antennas; Proceedings of, 2015, pp. 1–5.

[53] 3GPP, Study on 3D channel model for LTE, Tech. Rep. 36873, 3rd Generation Partnership Project (Jun 2015).

Alessandro Grassi is a Ph.D. student in information engineering at "Politecnico di Bari", Italy. He received a first level degree in electronics engineering in 2012 and a second level degree (cum laude) in telecommunications engineering in 2015. His research interests include 4G and 5G cellular networks, scheduling and QoS optimization in wireless networks, broadcasting in cellular networks, MIMO and Massive MIMO techniques, and random access protocols for cellular machine-to-machine communications. He is a core developer of the LTE-Sim simulator and he has been involved in the EU Horizon-2020 project "FANTASTIC-5G".

Giuseppe Piro is an Assistant Professor at "Politecnico di Bari", Italy. He received a first level degree and a second level degree (both cum laude) in Telecommunications Engineering from "Politecnico di Bari", Italy, in 2006 and 2008, respectively. He received the Ph.D. degree in Electronic Engineering from "Politecnico di Bari", Italy, on March 2012. His main research interests include quality of service in wireless networks, network simulation tools, 4G and 5G cellular systems, Information Centric Networking, nano communications, and Internet of Things. He founded both LTE-Sim and NANO-SIM projects and is a developer of Network Simulator 3. He has been involved in the following EU H2020 projects: FANTASTIC-5G, BONVOYAGE, symbIoTe. He is also regularly involved as member of the TPC of many prestigious international conferences.

Gennaro Boggia received, with honors, the Dr. Eng. Degree in Electronics Engineering in July 1997 and the Ph.D. degree in Electronics Engineering in March 2001, both from the Politecnico di Bari, Italy. Since September 2002, he has been with the Department of Electrical and Information Engineering at the Politecnico di Bari, Italy, where he is currently Associate Professor. From May 1999 to December 1999, he was visiting

researcher at the TILab, TelecomItalia Lab, Italy, where he was involved in the study of the Core Network for the evolution of 3G cellular systems. In 2007, he was visiting researcher at FTW (Vienna), where he was involved in activities on passive and active traffic monitoring in 3G networks. He has authored or co-authored more than 120 papers in international journals or conference proceedings, gaining more than 1000 citations. His research interests span the fields of Wireless Networking, Network Security, Cellular Communication, Information Centric Networking, Internet of Things (IoT), Protocol stacks for industrial applications, Internet measurements, Network Performance Evaluation. He is active in the IETF ICNRG working group and in the IEEE WG 6TiSCH. He is also regularly involved as member of the TPC of many prestigious international conferences. Currently, he serves as Associate Editor for the Springer Wireless Networks journal.

Martin Kurras received his Dipl.-Ing. (M.S.) degree in electrical engineering from the Technische University at Dresden, Desden Germany, in 2011. He joined the Fraunhofer Heinrich Hertz Institute (HHI) in October 2009. Currently he is working towards the Dr.-Ing. (Ph.D.) degree, where his topics of research are interference management and beamforming for positioning with a large number of antennas at one side (massive MIMO). Martin has co-/authored about 25 conference and journal papers in the area of mobile communications or antennas. He is a member of the System Level Innovation research group at Fraunhofer HHI.

Wolfgang Zirwas received his diploma degree in communication technologies in 1987 from Technical University of Munich (TUM). He started his work at the Siemens Munich central research lab for communication technologies with a focus on high frequency and high data rate TDM fiber systems for data rates up to 40 Gbit/s. He participated in several German and EU funded projects like COVERAGE, WINNER, Artist4G, METIS or Fantstic5G. Currently, he is at the end to end Lab of Nokia Bell Labs

in Munich investigating 5G mobile radio technologies.

Rakash SivaSiva Ganesan received the B.E. degree in electronics and communications engineering from the Mepco Schlenk Engineering College, affliated to Anna University, India, in 2006 and the M.Sc. degree from Technische Universitat Hamburg Harburg, Germany, in 2009. Currently he is pursuing his Ph.D. in relay aided interference alignment at the Communication Engineering Lab of Technische Universitat Darmstadt, Germany. His research interests include interference alignment, relaying and cooperative communication.

Klaus Pedersen received the M.Sc. degree in electrical engineering and the Ph.D. degree from Aalborg University, Aalborg, Denmark, in 1996 and 2000, respectively. He is currently leading the Nokia Bell Labs research team in Aalborg, and he is a part-time professor at Aalborg University in the Wireless Communications Network (WCN) section. He is the author/co-author of approximately 160 peer-reviewed publications on a wide range of topics, as well as an inventor on several patents. His current work is related to 5G New Radio, including radio resource management aspects, and the continued Long Term Evolution (LTE) and its future development, with special emphasis on mechanisms that offer improved end-to-end (E2E) performance delivery. He is currently part of the EU funded research project ONE5G that focuses on E2E-aware optimizations and advancements for the network edge of 5G New Radio. He is an IEEE Senior Member.

Lars Thiele is currently associated with the Fraunhofer Heinrich Hertz Institute, where he leads the System Level Innovation group. He received his Dipl.-Ing. (M.Sc.) degree in electrical engineering from Technische University Berlin in 2005 and his Dr.-Ing. (Ph.D.) degree from Technische Universität München in 2013. He has co- /authored more than 50 papers and

several book chapters in the fields of radio propagation modeling, large-scale system-level simulations, CoMP transmission, and massive MIMO.